Supplemental Material: Primal-Dual Coding to Probe Light Transport

Matthew O'Toole* University of Toronto
Ramesh Raskar† MIT Media Lab
Kiriakos N. Kutulakos* University of Toronto

1 Direct-Enhanced and Indirect-Only Probing Matrices

This section derives the direct-enhanced and indirect-only probing matrices from the stochastic diagonal estimator of Equation (6). Suppose $\mathbf{i}_+^k$ and $\mathbf{i}_-^k$ refer to the positive and negative components of a Rademacher vector $\mathbf{i}^k$, where $\mathbf{i}^k = \mathbf{i}_+^k - \mathbf{i}_-^k$. Note that the codes $\mathbf{i}_+^k$ and $\mathbf{i}_-^k$ have a Bernoulli distribution with success probability $p = 0.5$, where the elements have value 1 with probability p and value 0 with probability $1 - p$. The following derives from Equation (10):

$$\mathbf{i}^k(\mathbf{i}^k)^{\mathrm{T}} = \underbrace{[\mathbf{i}_+^k(\mathbf{i}_+^k)^{\mathrm{T}} + \mathbf{i}_-^k(\mathbf{i}_-^k)^{\mathrm{T}}]}_{\text{Direct-Enhancing Term}} - \underbrace{[\mathbf{i}_-^k(\mathbf{i}_+^k)^{\mathrm{T}} + \mathbf{i}_+^k(\mathbf{i}_-^k)^{\mathrm{T}}]}_{\text{Indirect-Only Term}} \quad (12)$$

The *direct-enhancing term* converges to a probing matrix containing the value 1 for diagonal elements, and the value 0.5 for off-diagonal elements. The *indirect-only term* converges to a matrix with 0 for diagonal elements and 0.5 for off-diagonal elements. As expected, subtracting the indirect-only probing matrix from the direct-enhanced matrix produces the identity matrix.

Random vectors $\mathbf{x}^k$ sampled from the Bernoulli distribution form the direct-enhanced matrix in the limit:

$$\mathbf{\Pi} = \lim_{K\to\infty} \frac{1}{K}\sum_{k=1}^{K} \mathbf{x}^k {\mathbf{x}^k}^{\mathrm{T}} \quad (13)$$

The diagonal entries $\mathbf{\Pi}_{nn}$ of the probing matrix have the following expected value:

$$\begin{aligned}\mathbf{\Pi}_{nn} &= \mathbb{E}[\frac{1}{K}\sum_{k=1}^{K} \mathbf{x}_n^k \mathbf{x}_n^k] \\ &= \frac{1}{K}\sum_{k=1}^{K} \mathbb{E}[(\mathbf{x}_n^k)^2] = p \end{aligned} \quad (14)$$

A similar derivation produces the expected value of the off-diagonal entries $\mathbf{\Pi}_{nm}$ where $n \neq m$:

$$\begin{aligned}\mathbf{\Pi}_{nm} &= \mathbb{E}[\frac{1}{K}\sum_{k=1}^{K} \mathbf{x}_n^k \mathbf{x}_m^k] \\ &= \frac{1}{K}\sum_{k=1}^{K} \mathbb{E}[\mathbf{x}_n^k \mathbf{x}_m^k] \\ &= \frac{1}{K}\sum_{k=1}^{K} \mathbb{E}[\mathbf{x}_n^k]\mathbb{E}[\mathbf{x}_m^k] = p^2 \end{aligned} \quad (15)$$

In the limit, the probing matrix has value p on the diagonal, and p^2 for off-diagonal elements. As the value p becomes smaller, the diagonal terms become larger relative to the off-diagonal terms.

*e-mail: {motoole,kyros}@cs.toronto.edu
†e-mail: raskar@media.mit.edu

The same set of random vectors $\mathbf{x}^k$, with a minor modification, forms the indirect-only probing matrix:

$$\mathbf{\Pi} = \lim_{K\to\infty} \frac{1}{K}\sum_{k=1}^{K} \mathbf{x}^k(\mathbf{1} - \mathbf{x}^k)^{\mathrm{T}} \quad (16)$$

The diagonal entries $\mathbf{\Pi}_{nn}$ of the probing matrix converge to the following:

$$\begin{aligned}\mathbf{\Pi}_{nn} &= \mathbb{E}[\frac{1}{K}\sum_{k=1}^{K} \mathbf{x}_n^k(1 - \mathbf{x}_n^k)] \\ &= \frac{1}{K}\sum_{k=1}^{K} \mathbb{E}[\mathbf{x}_n^k(1 - \mathbf{x}_n^k)] \\ &= \frac{1}{K}\sum_{k=1}^{K} (\mathbb{E}[\mathbf{x}_n^k] - \mathbb{E}[(\mathbf{x}_n^k)^2]) = 0 \end{aligned} \quad (17)$$

Once again, we derive the off-diagonal entries $\mathbf{\Pi}_{nm}$ where $n \neq m$ for the indirect-only probing matrix:

$$\begin{aligned}\mathbf{\Pi}_{nm} &= \mathbb{E}[\frac{1}{K}\sum_{k=1}^{K} \mathbf{x}_n^k(1 - \mathbf{x}_m^k)] \\ &= \frac{1}{K}\sum_{k=1}^{K} \mathbb{E}[\mathbf{x}_n^k(1 - \mathbf{x}_m^k)] \\ &= \frac{1}{K}\sum_{k=1}^{K} (\mathbb{E}[\mathbf{x}_n^k] - \mathbb{E}[\mathbf{x}_n^k]\mathbb{E}[\mathbf{x}_m^k]) \\ &= p(1-p) \end{aligned} \quad (18)$$

The off-diagonal term is maximum when $p = 0.5$. Note that, unlike the direct-enhanced case, there is no benefit in setting p to any other value.

When computing the direct-enhanced and indirect-only probing matrices, we generate the illumination and mask codes such that their sum produces a uniform image, as in the case of the direct-enhancing and indirect-only terms of Equation (12). This results in a set of mask codes that uniformly exposes each sensor pixel.

2 Accuracy of Stochastic Diagonal Estimator

Variance of estimate: derivation of Equation (7) The stochastic diagonal estimator converges to the diagonal matrix when using independent and identically distributed random vectors sampled from a distribution with mean 0 and variance 1. We derive the vari-

ance for a K-term estimate of the diagonal element $\mathbf{T}_{nn}$ as follows:

$$\begin{aligned} & Var((\mathbf{I} \odot \mathbf{T})\,\mathbf{1})_n \\ = \; & Var([\frac{1}{K}\sum_{k=1}^{K} \mathbf{i}^k \odot \mathbf{T}\,\mathbf{i}^k]_n) \\ = \; & Var(\frac{1}{K}\sum_{k=1}^{K}\sum_{m=1}^{M} \mathbf{i}_n^k \mathbf{i}_m^k \mathbf{T}_{nm}) \\ = \; & \frac{1}{K^2}\sum_{k=1}^{K} Var(\sum_{m=1}^{M} \mathbf{i}_n^k \mathbf{i}_m^k \mathbf{T}_{nm}) \\ = \; & \frac{1}{K} Var(\sum_{m=1}^{M} \mathbf{i}_n \mathbf{i}_m \mathbf{T}_{nm}) \\ = \; & \frac{1}{K}(\mathbb{E}[(\sum_{m=1}^{M} \mathbf{i}_n \mathbf{i}_m \mathbf{T}_{nm})^2] - \mathbb{E}[\sum_{m=1}^{M} \mathbf{i}_n \mathbf{i}_m \mathbf{T}_{nm}]^2) \\ = \; & \frac{1}{K}(\mathbb{E}[\sum_{m=1}^{M} \mathbf{i}_n^2 \mathbf{i}_m^2 \mathbf{T}_{nm}^2] - \mathbb{E}[\mathbf{i}_n^2 \mathbf{T}_{nn}]^2) \\ = \; & \frac{1}{K}(\mathbb{E}[\mathbf{i}_n^4 \mathbf{T}_{nn}^2] + \mathbb{E}[\sum_{\substack{m=1 \\ m\neq n}}^{M} \mathbf{i}_n^2 \mathbf{i}_m^2 \mathbf{T}_{nm}^2] - \mathbb{E}[\mathbf{i}_n^2 \mathbf{T}_{nn}]^2) \\ = \; & \frac{1}{K}(\mathbb{E}[\mathbf{i}_n^4]\mathbf{T}_{nn}^2 + \sum_{\substack{m=1 \\ m\neq n}}^{M} \mathbf{T}_{nm}^2 - \mathbf{T}_{nn}^2) \end{aligned} \tag{19}$$

Although any mean 0 and variance 1 distribution produces a probing matrix that converges to the identity matrix, the Rademacher sequence is optimal in the sense that the sequence minimizes the variance term. The variance is as follows for the Rademacher sequence:

$$\begin{aligned} & \frac{1}{K}(\mathbb{E}[\mathbf{i}_n^4]\mathbf{T}_{nn}^2 + \sum_{\substack{m=1 \\ m\neq n}}^{M} \mathbf{T}_{nm}^2 - \mathbf{T}_{nn}^2) \\ = \; & \frac{1}{K}(\mathbf{T}_{nn}^2 + \sum_{\substack{m=1 \\ m\neq n}}^{M} \mathbf{T}_{nm}^2 - \mathbf{T}_{nn}^2) \\ = \; & \frac{1}{K}\sum_{\substack{m=1 \\ m\neq n}}^{M} \mathbf{T}_{nm}^2 \end{aligned} \tag{20}$$

According to Equation (20), the number of primal-dual codes K must increase by a factor of 2 to decrease the variance by a factor of 2. Note that the variance term only depends on the off-diagonal matrix entries.

Frequency independence of estimate We show that the variance of the diagonal estimator is independent of the frequency of the off-diagonal elements. Suppose the off-diagonal elements follow a sinusoidal distribution with an integer frequency $f \in \{1, 2, \ldots, m-1\}$, as follows:

$$\mathbf{T}_{nm} = \sin((n-m)f\frac{\pi}{M}) \tag{21}$$

We compute the variance of the corresponding point to show frequency independence as follows:

$$\begin{aligned} \frac{1}{K}\sum_{\substack{m=1 \\ m\neq n}}^{M} \mathbf{T}_{nm}^2 &= \frac{1}{K}\sum_{\substack{m=1 \\ m\neq n}}^{M} \sin^2((n-m)f\frac{\pi}{M}) \\ &= \frac{1}{K}\sum_{m=1}^{M} \sin^2((n-m)f\frac{\pi}{M}) \\ &= \frac{1}{2K}[M - \sum_{m=1}^{M} \cos((n-m)f\frac{2\pi}{M})] \\ &= \frac{M}{2K} \end{aligned} \tag{22}$$

Note that the variance in Equation (22) is independent of the frequency f.

Photo quality versus number of codes We capture the same primal-dual photo multiple times using a variable number of codes. Figure 1 and Figure 2 illustrate how the quality of direct/indirect primal-dual photos depends on the number of codes used.

3 Codes Robust to Misalignments

Figure 3 illustrates how we handle spatial pixel misalignment. As explained in Section 4 of the paper, we define our codes $\mathbf{i}^{(k)}$ and $\mathbf{m}^{(k)}$ on a coarse pixel grid. Examples of such codes are shown in Figures 3(a),(b). However, using these codes directly may still result in artifacts near the boundary of coarse pixels. For this reason, we implement the code $\mathbf{i}^{(k)}$, $\mathbf{m}^{(k)}$ using a twelve-code sequence $(\mathbf{i}_l^{(k)}, \mathbf{m}_l^{(k)})$ that is defined on a finer pixel grid. Examples of this sequence are shown in Figures 3(c),(d). The result of using this sequence to implement $\mathbf{i}^{(k)}$, $\mathbf{m}^{(k)}$ is shown in Figures 3(e),(f). Note that although both Figures 3(a),(b) and Figures 3(e),(f) correspond to photos of the scene with the same code, artifacts no longer appear near coarse pixel boundaries in Figures 3(e),(f).

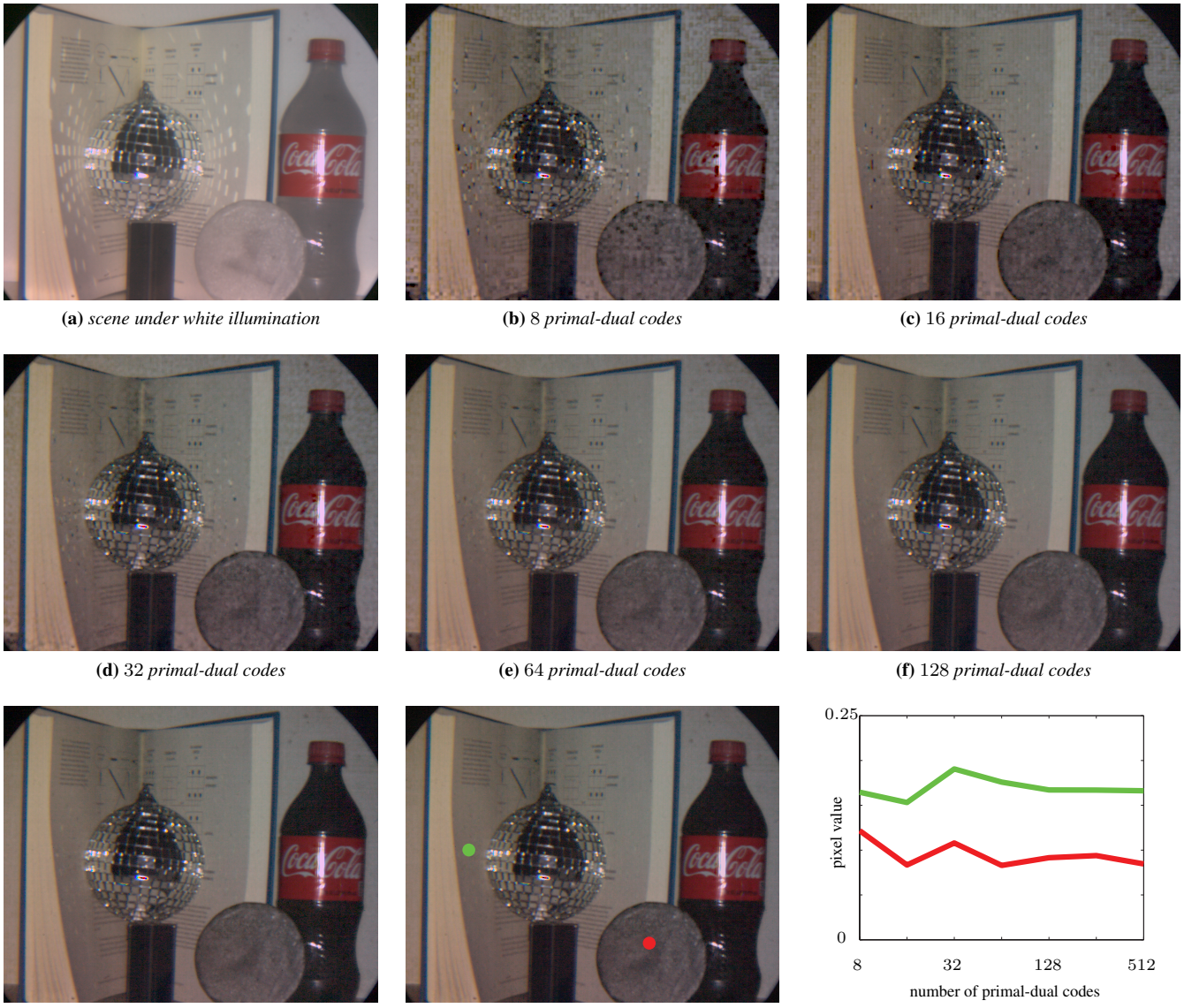

(a) *scene under white illumination*

(b) 8 *primal-dual codes*

(c) 16 *primal-dual codes*

(d) 32 *primal-dual codes*

(e) 64 *primal-dual codes*

(f) 128 *primal-dual codes*

(g) 256 *primal-dual codes*

(h) 512 *primal-dual codes*

(i)

Figure 1: ***(a)*** *Photo of a scene under white light, containing contributions from both direct and indirect illumination.* ***(b)-(h)*** *Effect of the number of primal-dual codes on the quality of the estimated direct illumination component. This component should not include specularities from the disco ball, subsurface scattering from the translucent wax disk and the milky water within the coke bottle, or from the inter-reflections of the book. With too few codes, the direct photos contain remnants of the primal-dual codes. These artifacts disappear for increased numbers of codes, at a rate defined by Equation (7).* ***(i)*** *Plot of the intensity of the estimated direct component at two scene points, as a function of the number of primal-dual codes: a point on a book lit by specular reflections from the disco ball (green) and a point on a wax disk that receives contributions from subsurface scattering (red). As the number of primal-dual codes increases, the intensities converge as expected.*

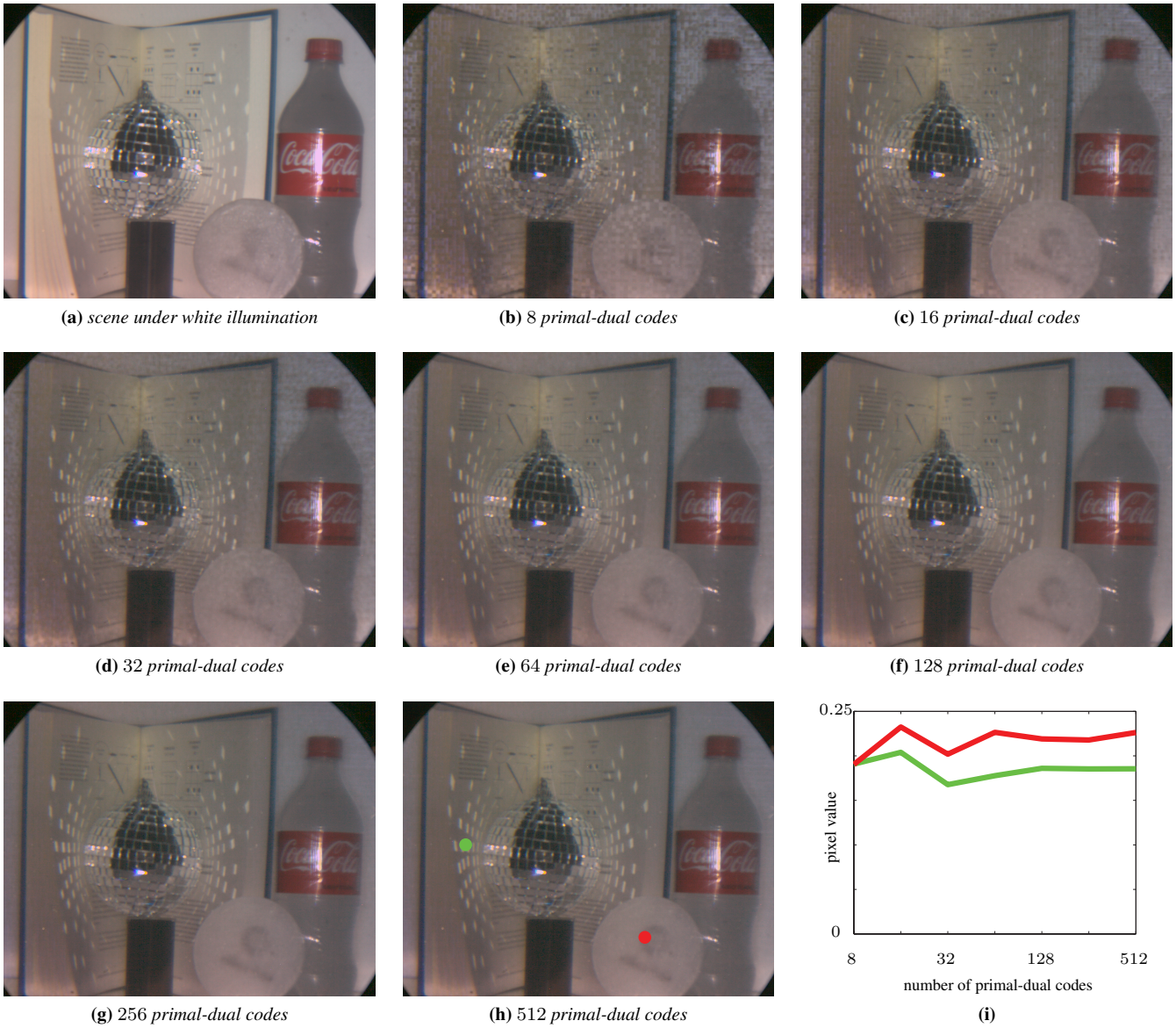

(a) *scene under white illumination*

(b) 8 *primal-dual codes*

(c) 16 *primal-dual codes*

(d) 32 *primal-dual codes*

(e) 64 *primal-dual codes*

(f) 128 *primal-dual codes*

(g) 256 *primal-dual codes*

(h) 512 *primal-dual codes*

(i)

Figure 2: ***(a)*** *Photo of the scene in Figure 1(a), shown again for reference.* ***(b)-(h)*** *Effect of the number of primal-dual codes on the quality of the estimated indirect illumination component.* ***(i)*** *Plot of the intensity of the indirect component at the same scene points as in Figure 1(i), as a function of the number of primal-dual codes. Once again, the plots for both points converge as expected.*

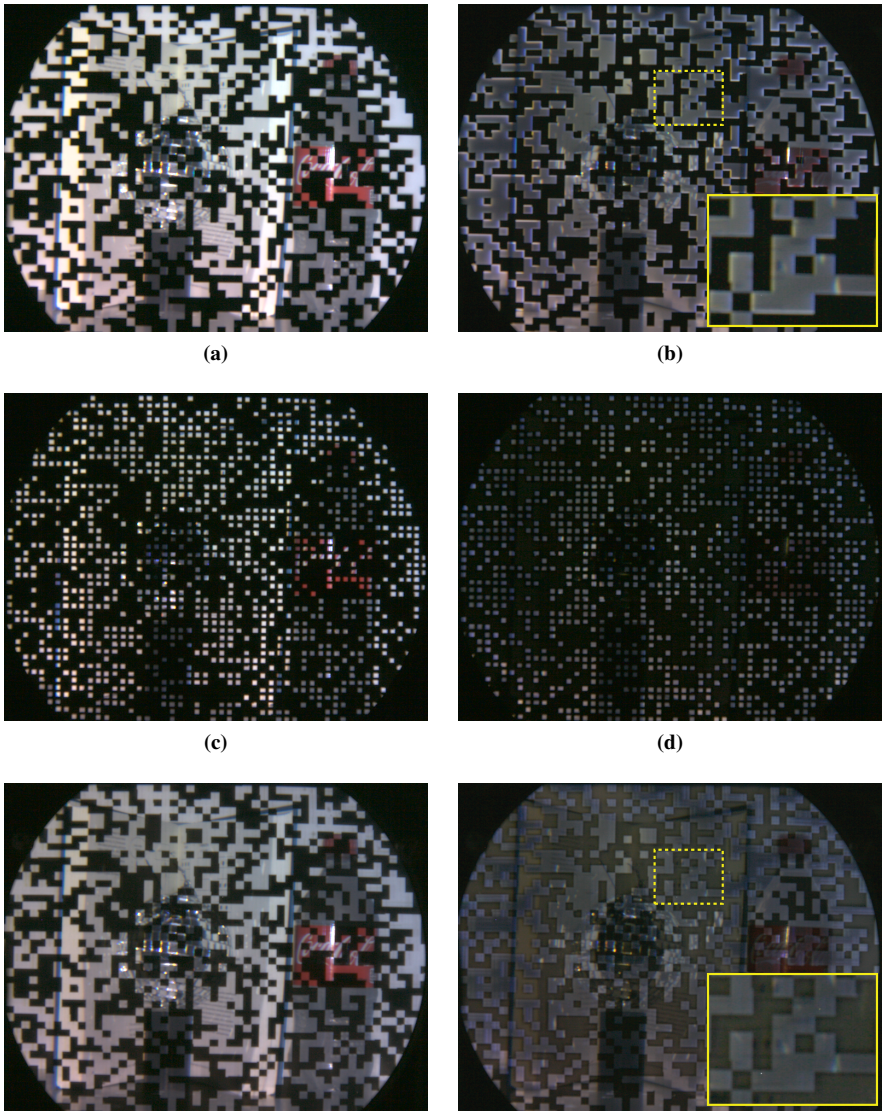

Figure 3: *Codes robust to pixel misalignment.* ***Row 1****: Images of a scene taken with a primal-dual code defined on a coarse pixel grid. The projector and mask patterns are identical in (a),* i.e., $\mathbf{i}^{(k)} = \mathbf{m}^{(k)}$*, whereas in (b) they are complements of each other. Misalignment artifacts appear as dark or bright pixels near coarse pixel boundaries. For example, the inset in (b) contains bright ghosting artifacts located near these boundaries, a result of the mask not blocking all direct light from the scene.* ***Row 2****: Photo of the scene corresponding to one member,* $(\mathbf{i}_l^{(k)}, \mathbf{m}_l^{(k)})$*, of the 12-code sequence we use to implement the codes in Row 1. Each code in the sequence samples the center* $\frac{1}{4}$*-th of each coarse pixel to avoid exposing the region near its boundary. The primal-dual code shown in Row 2 is shifted four times during the sequence. These shifts expose the area blocked by the previous codes in the sequence. The other eight codes in the sequence are blank frames captured with a mask consisting of all zeros.* ***Row 3****: Summing the photos corresponding to the* 12*-code sequence results in the photos shown in (e),(f). Note the lack of bright ghosting artifacts near the boundary of coarse pixels.*